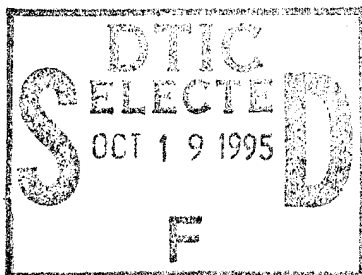# The Influence of Convection Velocity on the Turbulent Wall Pressure Wavenumber-Frequency Spectrum

William L. Keith
Bruce M. Abraham
Submarine Sonar Department

DTIC
SELECTED
OCT 1 9 1995
F

19951017 104

# Naval Undersea Warfare Center Division
## Newport, Rhode Island

DTIC QUALITY INSPECTED 8

# PREFACE

**Reviewed and Approved: 21 April 1995**

**R. J. Martin**
**Acting Head, Submarine Sonar Department**

# REPORT DOCUMENTATION PAGE

*Form Approved*
*OMB No. 0704-0188*

| 1. AGENCY USE ONLY (Leave Blank) | 2. REPORT DATE<br><br>21 April 1995 | 3. REPORT TYPE AND DATES COVERED<br><br>Final |
|---|---|---|

**4. TITLE AND SUBTITLE**

The Influence of Convection Velocity on the Turbulent Wall Pressure Wavenumber-Frequency Spectrum

**5. FUNDING NUMBERS**

**6. AUTHOR(S)**

William L. Keith and Bruce M. Abraham

**7. PERFORMING ORGANIZATION NAME(S) AND ADDRESS(ES)**

Naval Undersea Warfare Center
Detachment New London
New London, Connecticut 06320

**8. PERFORMING ORGANIZATION REPORT NUMBER**

TR 10,859

**9. SPONSORING/MONITORING AGENCY NAME(S) AND ADDRESS(ES)**

**10. SPONSORING/MONITORING AGENCY REPORT NUMBER**

**11. SUPPLEMENTARY NOTES**

**12a. DISTRIBUTION/AVAILABILITY STATEMENT**

Approved for public release; distribution is unlimited.

**12b. DISTRIBUTION CODE**

**13. ABSTRACT (Maximum 200 words)**

Cross-spectral and cross-correlation data from experiments and numerical simulations have shown the turbulent wall pressure convection velocity to vary with the streamwise spatial separation $\xi$, due to the spatial decay rates of turbulent structures in the inner and outer regions of the boundary layer. This effect is shown to have a significant impact on the distribution of energy in the wavenumber-frequency spectrum $\Phi(k_1,\omega)$. The overprediction of spectral levels at low wavenumbers using the standard Corcos model is shown to result from assuming a constant convection velocity in the cross spectrum. The spectral levels at subconvective and lower wavenumbers are shown to be directly influenced by the decay and convection of turbulence in both the inner and outer regions of the boundary layer. These results compare favorably with recent numerical results. The attenuations in the autospectrum due to finite diameter sensors are shown not to be significantly influenced by this effect. Convection velocity measurements from past investigations that cover the range $285 \le R_\theta \le 29{,}000$ are compared, and an outer variable scaling is found to be the most effective for collapsing the data.

**14. SUBJECT TERMS**
Convection Velocity, Cross Correlation, Cross Spectrum, Spatial Separation, Streamwise Wavenumber, Turbulent Wall Pressure, Wavenumber-Frequency Spectrum

**15. NUMBER OF PAGES**
32

**16. PRICE CODE**

| 17. SECURITY CLASSIFICATION OF REPORT | 18. SECURITY CLASSIFICATION OF THIS PAGE | 19. SECURITY CLASSIFICATION OF ABSTRACT | 20. LIMITATION OF ABSTRACT |
|---|---|---|---|
| UNCLASSIFIED | UNCLASSIFIED | UNCLASSIFIED | SAR |

# TABLE OF CONTENTS

# LIST OF ILLUSTRATIONS

# LIST OF TABLES

# LIST OF NOMENCLATURE

$G(\xi,\eta,\omega)$ — Cross Spectrum ($\mu Pa^2/(rad/sec)$)

$K_1 = -k_1\delta^*$ — Streamwise Wavenumber (nondimensional)

$K_2 = k_2\delta^*$ — Spanwise Wavenumber (nondimensional)

$K_c = \Omega/U_c = k_c\delta^*$ — Convective Wavenumber (nondimensional)

$R = r/\delta^*$ — Pressure Sensor Radius (nondimensional)

$R_\tau = u_\tau\delta/\nu$ — Ratio of the Outer to Inner Length Scale

$R_\theta = U_o\theta/\nu$ — Momentum Thickness Reynolds Number

$T(\xi,\eta,r)$ — Sensor Correlation Function ($cm^{-2}$)

$U_c = u_c/U_o$ — Nondimensional Convection Velocity

$U_o$ — Freestream Velocity (m/sec)

$u_\tau = (\tau/\nu)^{1/2}$ — Friction Velocity (m/sec)

$X = \xi/\delta^*$ — Nondimensional Streamwise Separation

$Z = \eta/\delta^*$ — Nondimensional Spanwise Separation

$\delta$ — Boundary Layer Thickness (cm)

$\delta^*$ — Boundary Layer Displacement Thickness (cm)

$\nu$ — Fluid Kinematic Viscosity ($cm^2/sec$)

$\rho$ — Fluid Density ($gm/cm^3$)

$\theta$ — Boundary Layer Momentum Thickness (cm)

$\tau$ — Mean Wall Shear Stress ($nt/m^2$)

$\gamma,\beta$ — Corcos Model Decay Parameters (streamwise and spanwise)

$\omega$ — Radial Frequency

# LIST OF NOMENCLATURE (CONT'D)

$\phi(\xi,\omega)$            Cross-Spectrum Phase (rad)

$\Phi^*(\Omega) = \Phi(\omega)/\rho^2\delta^*U_o^3$        Autospectrum (nondimensional)

$\Omega = \omega\delta^*/U_o$          Nondimensional Frequency

$\Phi^*(K_1,\Omega) = \Phi(k_1,\omega)2\pi/\Phi(\omega)\delta^*$      Wavenumber-Frequency Spectrum (nondimensional and normalized)

$$\text{where} \quad 1/2\pi \int_{-\infty}^{\infty} \Phi^*(K_1,\Omega)dK_1 = 1$$

$\Phi^*(K_1,K_2,\Omega) = \Phi(k_1,k_2,\omega)4\pi^2/\Phi(\omega)\delta^{*2}$   Wavenumber-Frequency Spectrum (nondimensional and normalized)

$$\text{where} \quad 1/4\pi^2 \int_{-\infty}^{\infty} \Phi^*(K_1,K_2,\Omega)dK_1dK_2 = 1$$

iv

# THE INFLUENCE OF CONVECTION VELOCITY ON THE TURBULENT WALL PRESSURE WAVENUMBER-FREQUENCY SPECTRUM

## INTRODUCTION

Empirically derived models of the turbulent wall pressure wavenumber-frequency spectrum are required in problems of flow-induced vibration and noise. Of particular interest is the energy in the subconvective and low-wavenumber region, which excites the lower order vibrational modes of structures. A direct measurement of $\Phi(k_1,k_2,\omega)$ requires an array of many closely spaced sensors from which data are acquired simultaneously in time. Due to the extensive number of sensors and signal processing required, very few such measurements have been made in experimental flow facilities. The inherent problem of spatial aliasing due to sensor spacing limits the wavenumber and frequency bandwidths of the measurements, as discussed by Keith and Abraham (1994). Models of $\Phi(k_1,k_2,\omega)$ are therefore often derived from measurements of the cross spectrum made with a relatively small number of sensors. Uncertainties result from the limited number of spatial separations as well as from the size of the pressure sensors, which determines the separations that are possible.

A convection or phase velocity, $u_c$, may be determined from the streamwise cross-spectrum phase $\phi(\xi,\omega)$ by use of the relationship $\phi(\xi,\omega) = \omega\xi/u_c$. It is commonly assumed in estimating the wavenumber-frequency spectrum that $u_c$ is independent of $\xi$. In fact, $u_c$ varies with $\xi$ due to the variation in convection velocities and spatial decay rates of the pressure-producing turbulent structures in the inner and outer regions of a turbulent boundary layer. Here, we first formulate the problem in the spatial domain using the Corcos (1963) cross-spectrum model. We then compare experimental and numerical data for $u_c$ from investigations covering a wide range of Reynolds numbers in order to determine effective scaling parameters. The wavenumber-frequency spectra are next estimated by transforming the cross spectrum, taking into account the dependence of $u_c$ upon $\xi$. Comparisons with recent numerical results are shown to be favorable, and the effects on the attenuations in the autospectra due to finite sensor size are determined.

## MODELING THE WALL PRESSURE CROSS SPECTRUM

The streamwise wall pressure cross spectrum may be expressed as

$$G(\xi,\omega) = |G(\xi,\omega)|\, e^{-i\phi(\xi,\omega)} . \tag{1}$$

For a fixed frequency $\omega_0$, assuming $u_c$ is independent of $\xi$ and $|G(\xi,\omega_0)|$ decays exponentially with $\xi$, equation (1) becomes

$$G(\xi,\omega_0) = \Phi(\omega_0)e^{(\alpha|\xi|-i\omega_0\xi/u_c(\omega_0))} , \tag{2}$$

where $\alpha$ is a decay constant. The spectrum $\Phi(k_1,\omega_0)$ is then

$$\Phi(k_1,\omega_0) = \Phi(\omega_0)/2\pi \int_{-\infty}^{\infty} e^{(\alpha|\xi|-i(k_1 + \omega_0/u_c(\omega_0))\xi)}d\xi . \tag{3}$$

Using MACSYMA (Rand 1984), we obtain the closed-form solution

$$\Phi(k_1,\omega_0) = (\Phi(\omega_0)/2\pi)(-2\alpha/(\alpha^2 + (k_1 + k_c)^2)) . \tag{4}$$

If $u_c$ is allowed to vary with $\xi$ as well as $\omega_0$ in equation (3), a spatial modulation of the phase term results, and in general the integral cannot be evaluated in closed form. Assuming $u_c$ to be independent of $\xi$, we define $\alpha = \gamma\,\omega_0/u_c(\omega_0)$, and express equation (2) in terms of the similarity variable $\xi^* = \omega_0\xi/u_c(\omega_0)$ such that

$$G(\xi^*,\omega_0) = \Phi(\omega_0)e^{(\gamma|\xi^*|-i\,\xi^*)} . \tag{5}$$

The Corcos (1963) cross-spectrum model is separable in the streamwise and spanwise coordinates. Equation (5) represents the streamwise component of the model. Recently Farabee and Casarella (1991) and Keith and Barclay (1993) have shown that the similarity scaling holds over a limited frequency range. Although Corcos did not transform his cross-spectrum model to the wavenumber domain, equation (4) with $\alpha$ replaced by $\gamma k_c$ is commonly referred to as the Corcos model of $\Phi(k_1,\omega_0)$. Corcos defined a convection velocity in terms of the phase of the cross spectrum, and stated that "$u_c$ is found to be a function of $\omega$ and to be almost independent of $\xi$ and $\eta$." This conclusion was likely based upon the limited amount of convection velocity data available at that time.

Farabee and Casarella (1991) showed that the similarity scaling proposed by Corcos was effective for collapsing their cross-spectral data, taking into account the variation of $u_c$ with $\xi$. However, the influence of the variation of $u_c$ with $\xi$ on the wavenumber-frequency spectrum has not been investigated to date. A criticism of the model for $\Phi(k_1,\omega_0)$ given by equation (4) is an apparent overprediction of spectral levels at subconvective and lower wavenumbers. Here, higher

2

spectral levels in these regions will be shown to result from constraining $u_c$ to be constant when transforming the cross spectrum. Taking into account the variation of $u_c$ with $\xi$ will be shown to lead to improved estimates of $\Phi(k_1,\omega_0)$.

## COMPARISON OF WALL PRESSURE CONVECTION VELOCITIES

The dependence of the convection velocity on the spatial separation and effective scaling laws will be determined by comparisons of previous measurements. The dominant trend in the data is an increase in $u_c(\xi,\omega)$ as $\xi$ increases and $\omega$ decreases. This results from the locations of the wall-pressure-producing turbulent structures in the boundary layer as well as from their rate of spatial decay. The larger structures at locations farther from the wall convect faster and are coherent over larger distances than those near the wall. For larger separations, the contributions from the larger structures therefore dominate $u_c(\xi,\omega)$. At smaller separations, the contributions from the smaller structures coherent over those distances cause a reduction in $u_c(\xi,\omega)$. The increase in $u_c(\xi,\omega)$ with decreasing $\omega$ is also consistent with these effects.

Here we focus on the spatial variation of $u_c$ for discrete, narrowband, and broadband frequency ranges. We compare data from six investigations that cover two orders of magnitude in $R_\theta$. The data of Farabee and Casarella (1991) were determined from the phase of the cross spectrum at discrete frequencies; those of Willmarth and Wooldridge (1962) and Keith et al. (1991) were determined from narrowband correlation measurements; and those of Choi and Moin (1990), Schloemer (1967), and Bull (1967) from broadband correlation functions. Farabee and Casarella (1991) determined scaling laws for wall pressure autospectra and the regions of the boundary layer that contribute at particular frequency ranges. Use of these length and time scales results in scalings given by $u_c/U_0$ vs. $\xi/\delta^*$, $u_c/u_\tau$ vs. $\xi/\delta$, and $u_c/u_\tau$ vs. $\xi u_\tau/\nu$.

For comparing the data using the outer scaling $u_c/U_0$ vs. $\xi/\delta^*$, we consider the frequency bands scaled as $\omega\delta^*/U_0$. The higher discrete frequency of Farabee and Casarella falls at the center of the narrow bandwidth of Keith et al. (at both $R_\theta$). These data display a reasonable collapse, as shown in figure 1. Although the narrow bandwidth of Willmarth and Wooldridge lies above the higher discrete frequency of Farabee and Casarella, these data collapse well. The numerical simulation of Choi and Moin covers approximately the same broad band as Bull's. Choi and Moin's data are above Bull's at the lower separations, but converge at the higher. The broadband data of Schloemer and Bull agree well where Schloemer's data covers a slightly higher frequency range than do Bull's. The low discrete frequency of Farabee and Casarella lies within the broad band of Bull. The two data sets agree well for the larger separations. This agreement between broadband

and discrete low-frequency data reflects the inherent filtering of the higher frequency contributions in the broadband data resulting from the spatial separations of the sensors.

The outer scaling effectively collapses the discrete, narrowband and broadband data sets. The dominant trend of increasing convection velocity with increasing separation is apparent. We investigated the use of $\delta$ rather than $\delta^*$ as an outer length scale, and found no significant effect. At low values of $\xi/\delta^*$, the data sets at higher $R_\theta$ tend to display a sharper roll-off than Farabee and Casarella's low-frequency data. For the scaling $u_c/u_\tau$ vs. $\xi/\delta$ of figure 2, we consider the frequency bands scaled as $\omega\delta/u_\tau$. Although the higher discrete frequency data of Farabee and Casarella fall at the center of the narrow bands of Keith et al. at both $R_\theta$, these data do not collapse well. In addition, the collapse of the data of Keith et al., which covers the same narrow band at both $R_\theta$, is poor, with the lower $R_\theta$ data lying below the higher. Bull and Schloemer's broad bands are comparable, and the two data sets collapse fairly well, with Schloemer's data slightly below Bull's. Choi and Moin's broad band covers the lower half of Bull's, but their data lies significantly below Bull's. The use of $u_\tau$ as a velocity scale combined with an outer length scale therefore does not effectively collapse data over a wide range of $R_\theta$. Data at lower $R_\theta$ are mapped below the higher $R_\theta$ data, resulting in the trend of increasing levels with increasing $R_\theta$.

The use of $u_\tau$ as a velocity scale combined with the inner length scale, $v/u_\tau$, leads to an improved collapse of the data of figure 2, as shown in figure 3. For this inner scaling, we consider the frequency bands scaled as $\omega v/u_\tau^2$. The low discrete frequency data of Farabee and Casarella fall at the center of the narrow band of Keith et al. at the higher $R_\theta$. These data collapse well. The high discrete frequency data of Farabee and Casarella falls at the center of the narrow band of Willmarth and Wooldridge. The Willmarth and Wooldridge data lie above those of Farabee and Casarella. Choi and Moin's broadband data extend to significantly higher frequencies, $\omega v/u_\tau^2$, than the other data sets. Their data lies significantly below those of the other three investigations. Although Schloemer's data covers a somewhat higher frequency range than do Bull's, their data collapse fairly well. The data of Farabee and Casarella (low $\omega$), Bull, Keith et al. (high $R_\theta$), and Willmarth and Wooldridge collapse well at larger values of $\xi u_\tau/v$.

The outer variable scaling of figure 1 collapses all of the data sets over two orders of magnitude in $R_\theta$ somewhat more effectively than does the inner variable scaling. Based upon the analysis of Farabee and Casarella (1991), in view of the frequency bands as given in table 1, contributions to the wall pressure autospectra for these cases are from a significant or entire portion of the log-law region. The effectiveness of outer and inner variables for collapsing the convection velocity data is consistent with the sources existing in the log-law region.
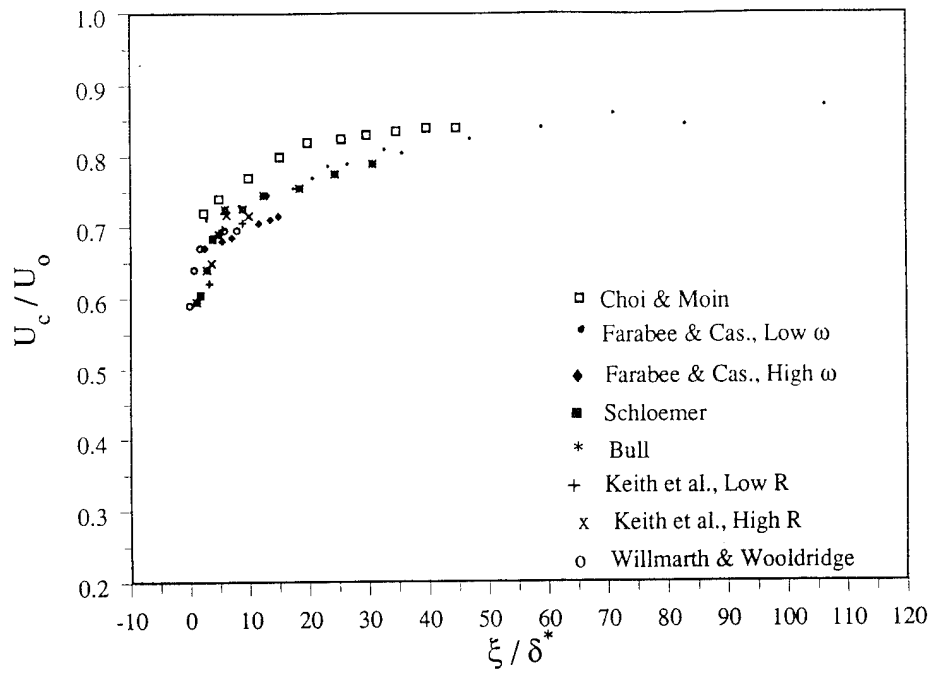
4

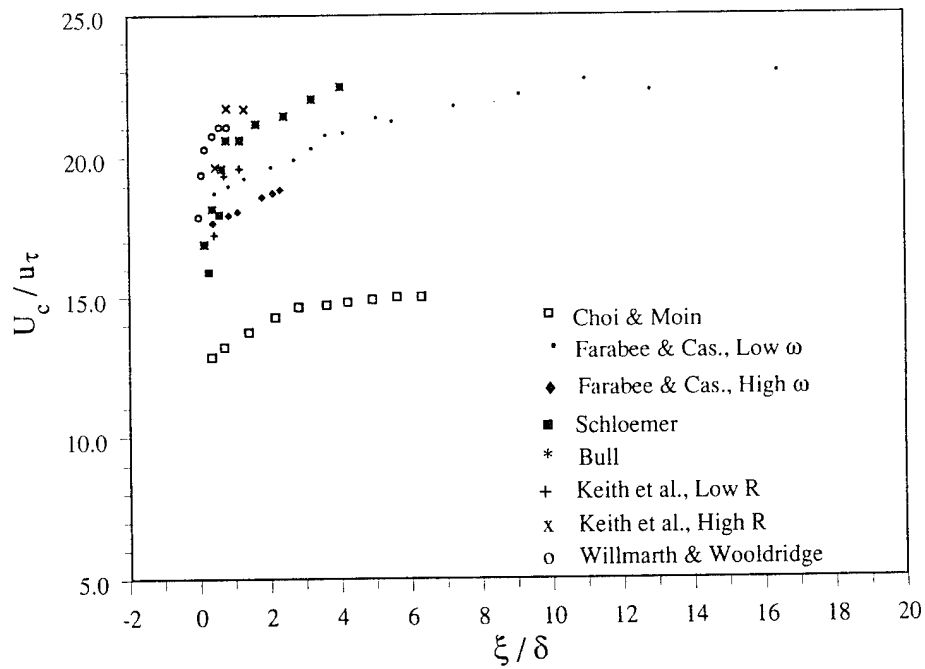Figure 1. Comparison of Convection Velocities Scaled With Outer Variables



Figure 2. Comparison of Convection Velocities Scaled With Mixed Variables

Table 1. Parameters for Comparison of Convection Velocity Data

| Investigation | $R_\theta$ | $R_\tau$ | $\omega\delta^*/U_o\vert_1$ | $\omega\delta^*/U_o\vert_2$ | $\omega\delta/u_\tau\vert_1$ | $\omega\delta/u_\tau\vert_2$ | $\omega\nu/u_\tau^2\vert_1$ | $\omega\nu/u_\tau^2\vert_2$ | Region |
|---|---|---|---|---|---|---|---|---|---|
| Choi & Moin (1990), $R(\xi,\tau)$, Broad Band | 285 (DNS) | 180 | 0.08 | 3.55 | 10.00 | 450.00 | 0.055 | 2.484 | mid-high |
| Farabee & Casarella (1991), $\Phi(\xi,\omega)$ Narrow Band | 3,400 (air) | 1,165 | 0.24  0.96 | ----  ---- | 40.8  163.0 | ----  ---- | 0.035  0.140 | ----  ---- | mid  log-law |
| Schloemer (1967),$R(\xi,\tau)$ Broad Band | 5,800 (air) | 2,043 | 0.115 | 7.655 | 20.772 | 1,384.83 | 0.010 | 0.678 | mid-high |
| Bull (1967), $R(\xi,\tau)$ | 10,000 (air) | 3,614 | 0.038 | 4.08 | 8.24 | 884.30 | 0.002 | 0.245 | mid- log law |
| Keith et al. (1991), $R(\xi,\tau)$ Narrow Band | 11,700  21,700 (water) | 4,182  6,778 | 0.47  0.46 | 1.41  1.42 | 100.09  106.29 | 300.28  328.11 | 0.024  0.016 | 0.072  0.048 | log-law  log-law |
| Willmarth & Wooldridge (1962), $R(\xi,\tau)$, Narrow Band | 29,000 (air) | 10,560 | 4.10 | 6.80 | 1,222.80 | 2,028.10 | 0.116 | 0.193 | log-law |
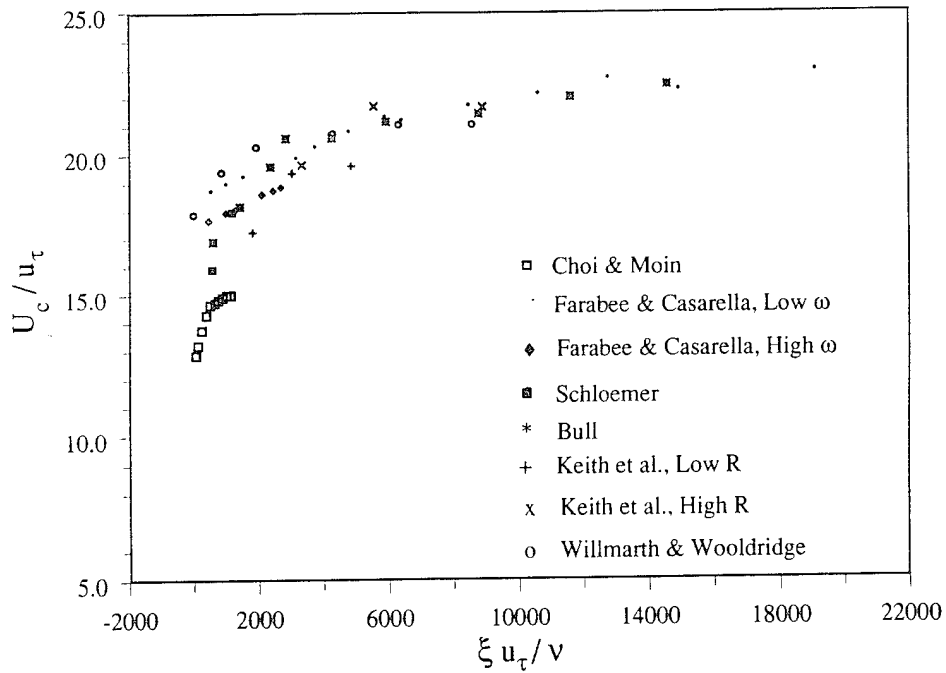


Figure 3. Comparison of Convection Velocities Scaled With Inner Variables

6

# ESTIMATED WAVENUMBER-FREQUENCY SPECTRUM $\Phi^*(K_1,\Omega)$

Defining nondimensional outer variables $X = \xi/\delta^*$, $K_1 = -k_1\delta^*$, $U_c = u_c(\omega_0,\xi)/U_o$, $\Omega = \omega_0\delta^*/U_o$, and $K_c = \Omega/U_c$, a nondimensional normalized form of the Corcos model is given by

$$\Phi^*(K_1,\Omega) = (-2\gamma/K_c)(1/(\gamma^2 + (1 - K_1/K_c)^2)) \ . \tag{6}$$

If the dependence of the convection velocity on spatial separation is taken into account, the spectrum may be evaluated as

$$\Phi^*(K_1,\Omega) = \int_{-\infty}^{\infty} e^{(\gamma|\Omega X/U_c(X)|-i(-K_1 + \Omega/U_c(X))X)}dX \ . \tag{7}$$

The sign of $K_1$ was chosen as negative (in defining nondimensional variables) to place the convective ridge at positive $K_1$. A value for the decay constant $\gamma$ of -0.145 provided an accurate exponential curve fit to the magnitude of Farabee and Casarella's (1991) cross spectrum for $\Omega = 0.24$. A function of the form $U_c(X) = aX^b$ was fit to the low-frequency data of Farabee and Casarella (1991), resulting in a standard deviation of 0.04. For $X > 81$, $U_c(X)$ was taken as constant at 0.85. This curve-fit results in a sharper roll-off near the origin than that supported by Farabee and Casarella's data, and more accurately models the broadband data of Bull and the higher frequency data of Willmarth and Wooldridge, as shown in figure 4. The function $U_c(X) = a(X+1)^b$ resulted in the same standard deviation of 0.04 for Farabee and Casarella's low-frequency data, and gives a value for $U_c(0)$ of 0.645, which agrees with that estimated by Farabee and Casarella.

Equation (7) was evaluated numerically, with $U_c(X) = aX^b$. The resulting spectrum of figure 5 exhibits significantly lower levels at subconvective and lower wavenumbers and increased levels at higher wavenumbers, in comparison to the Corcos model given by equation (6) with a constant value of 0.85 for $U_c$. The function $U_c(X) = a(X+1)^b$ leads to the same trends in the spectrum as the former, with the effects slightly diminished. For comparison, we also considered the function $a(X+10)^b$ with less of a roll-off near the origin. This function produced the same trends in the spectrum, with the effects further diminished. A fifth-order polynomial (not shown here) was also fit to the data of Farabee and Casarella, and resulted in a spectrum that agreed quite well with that obtained using the function $a(X+1)^b$. The function $a(X+1)^b$ was found to most accurately model the convection velocity data and provides the best estimate of the wavenumber-frequency spectra for this case.
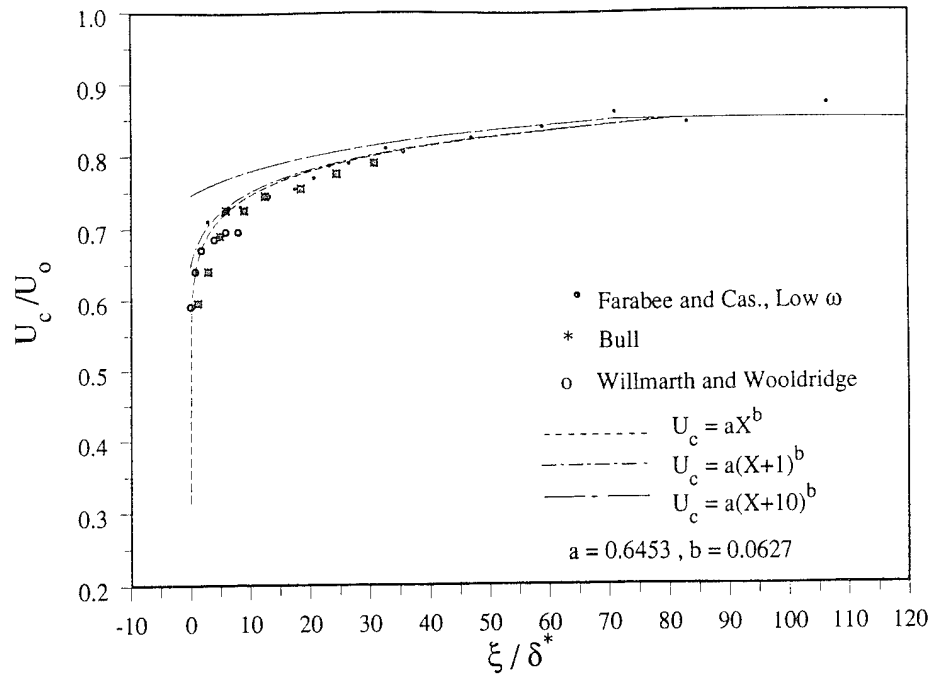
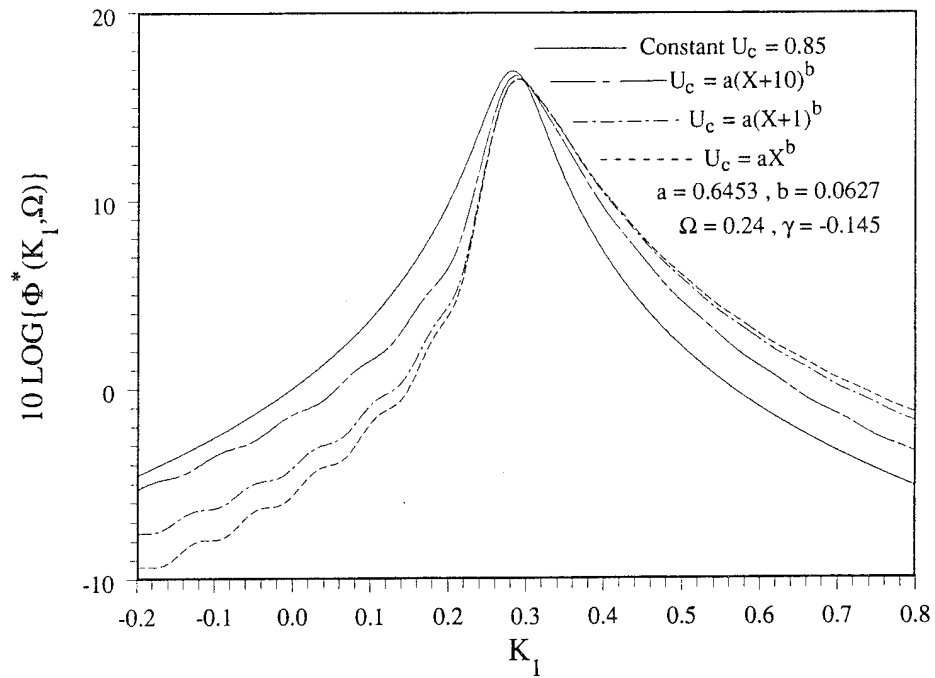Figure 4. Curve Fits to Convection Velocity Data



Figure 5. Effects of the Roll-Off of $U_c(X)$ for Small X on the
Wavenumber-Frequency Spectrum $\Phi^*(K_1,\Omega)$

8

Comparison of the cases $aX^b$ and $a(X+1)^b$ provides insight into the sensitivity of the spectrum to small-scale turbulence. The roll-off of $U_c(X)$ near the origin results from small-scale turbulent structures with lower convection velocities and rapid spatial decay. For $X \geq 1$, the values for $U_c(X)$ given by $aX^b$ and $a(X+1)^b$ agree to within 5 percent. The differences in the roll-off of $U_c(X)$ for $0 < X < 1$ therefore lead to the differences in the spectra at low wavenumbers, with the sharper roll-off leading to lower levels. For the boundary layer of Farabee and Casarella, $X = 1$ corresponds to $\xi = 188\nu/u_\tau$. A decay constant of 0.145 implies that a turbulent pressure-producing structure loses 84 percent of its coherence as it convects and decays over $2\lambda$. A cut-off may then be defined as $\lambda < 100\nu/u_\tau$ for turbulence that influences $U_c(X)$ only over this particular spatial range.

At the low frequency $\omega\delta^*/U_O = 0.24$, $\lambda = 3.5\delta^*$ at the convective wavenumber and the primary energy in $\Phi(\omega)$ results from turbulence activity in the outer region of the boundary layer. However, the spectral levels at wavenumbers above and below the convective ridge are directly influenced by the small-scale turbulence. The primary energy in small-scale turbulence with $\lambda < 100\nu/u_\tau$ exists at high convective wavenumbers, $k_c\nu/u_\tau > 0.06$, and corresponding high frequencies, $\omega\nu/u_\tau^2 > 1.0$. Farabee and Casarella concluded that energy at $\omega\nu/u_\tau^2 > 0.3$ results from small-scale turbulence activity in the buffer region of the boundary layer. Such small-scale turbulence has little effect on the total energy in the autospectrum $\Phi(\omega)$ at low frequencies, but significantly influences the distribution of energy in the wavenumber-frequency spectrum at low frequencies. This conclusion is also consistent with that of Farabee (1986). By considering the spectral solution to the Poisson equation, he concluded that contributions (of various levels) to $\Phi(\omega)$ at low frequencies are possible from turbulent velocity fluctuations throughout the entire boundary layer.

Control of the small-scale turbulence could therefore lead to improvements in flow-induced vibrations and noise by reducing the low-wavenumber spectral levels. A sharper roll-off for small separations was shown to result in lower spectral levels at low wavenumbers. Control aimed at reducing the convection velocities of the small-scale structures could therefore lead to this effect. However, changes in the spatial decay as well as in the inherent coupling between the inner and outer regions of the boundary layer will clearly have an impact. Our results also emphasize the requirement for extremely small pressure sensors of diameter $25\nu/u_\tau$ or less to accurately measure the convection velocities at very small spatial separations.

The effect of the convection velocities of the large-scale structures on the spectrum was also determined by varying the constant value of $U_c(X)$ at large separations. The largest value of

9

$U_c(X)$ for Farabee and Casarella's low-frequency data was 0.87 at X = 106. Use of the function $a(X+1)^b$, a constant value of 0.87 for X > 105 rather than 0.85 for X > 80 had a negligible effect on the spectrum. Using a lower value of 0.80 for X > 29 had a very small effect on the convective and higher wavenumbers. However, at subconvective and lower wavenumbers, the spectral levels display an apparent oscillation as shown in figure 6. These oscillations thus result from changes in $U_c(X)$ for X > 29. For Farabee and Casarella's boundary layer, X = 29 corresponds to $\xi$ = 5,460$v/u_\tau$, or 4.7$\delta$. Structures with $\lambda$ < 2,730$v/u_\tau$ or $\lambda$ < 2.3$\delta$ have a negligible influence on $U_c(X)$ for X > 29. The convection velocities of turbulence with $\lambda$ > 2.6$\delta$ in the outer region therefore also influence the spectrum at subconvective and lower wavenumbers. For comparison, we also considered a constant value of 0.75 for $U_c(X)$ for X > 9. This leads to a shift of the convective ridge to higher wavenumbers. The shape of the spectrum agrees with the model of equation (6) as expected, since $U_c(X)$ is constant over a large spatial region.

The sensitivity of the spectrum to the decay constant $\gamma$ was determined for -0.165 $\leq \gamma \leq$ -0.110, with $U_c(X) = a(X+1)^b$. At the convective ridge, the levels increase as $|\gamma|$ decreases, as shown in figure 7. At higher wavenumbers, the levels decrease slightly as $|\gamma|$ decreases. At subconvective and low wavenumbers, the levels decrease significantly as $|\gamma|$ decreases, with oscillations similar to those obtained by decreasing the constant value of $U_c$ at large separations. The value of -0.145 corresponds to the data of Farabee and Casarella at $\Omega$ = 0.24, and the value of -0.125, which is accurate at higher frequencies, is commonly used for modeling purposes. Although a value of -0.110 does not support the data at this frequency, the resulting oscillations in the spectral levels at subconvective and low wavenumbers are interesting. Whether such oscillations are physically realizable or simply result from an inaccurate curve fit to the data is not clear at the present time.

Keith and Barclay (1993) investigated the effects of a large eddy breakup device (LEBU) on the wall pressure cross spectra. The LEBU caused no measurable changes in the convection velocities, but led to a significant loss of coherence and greater spatial decay at low frequencies. Reductions in the autospectral levels also occurred at low frequencies. Using the model given here by equation (4), they found the normalized wavenumber-frequency spectrum had reduced levels at the convective ridge and increased levels at lower and higher wavenumbers. The results of figure 7 support the same trends, although the shapes of the spectra are different due to the variation of convection velocity with separation. Keith (1989) investigated the effect of riblets on the wall pressure cross spectra. The riblets produced no measurable change in the convection velocities or the autospectra, but led to increased coherence levels, implying reduced spatial decay at low frequencies. The results of figure 7 indicate that riblets may therefore lead to increased levels near the convective ridge and reduced levels at subconvective and low wavenumbers.
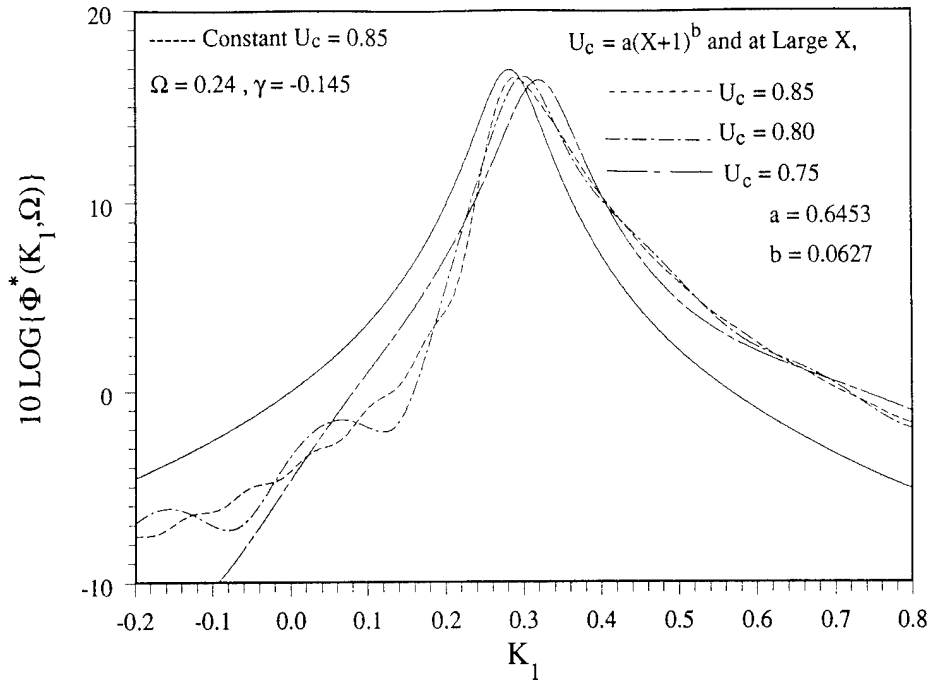
10

Figure 6. Effects of the Value of $U_c(X)$ for Large X on the
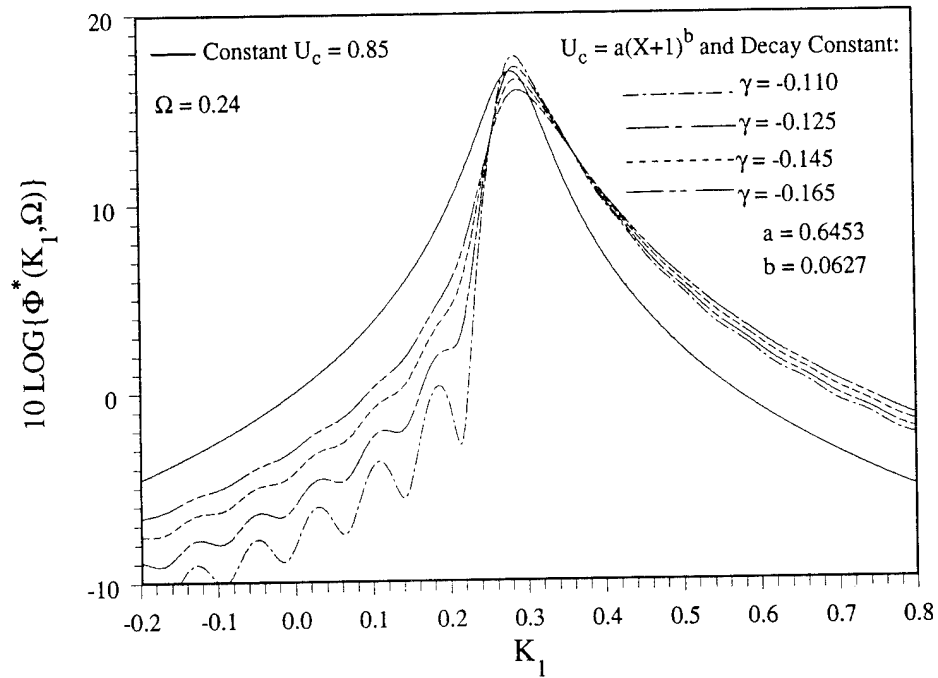Wavenumber-Frequency Spectrum $\Phi^*(K_1,\Omega)$



Figure 7. Effects of the Exponential Decay Constant on the
Wavenumber-Frequency Spectrum $\Phi^*(K_1,\Omega)$

11

Recent numerical simulations of low Reynolds number fully developed channel flow provide a detailed description of the space-time wall pressure field. The characteristics of the streamwise wavenumber-frequency spectra computed from these simulations were recently discussed by Chang et al. (1994). The Direct Numerical Simulation "DNS3" (with $R_\tau$ = 180) and Large Eddy Simulation "LES2" (with $R_\tau$ = 171) results of Chang et al. (1994) for frequency $\Omega$ = 0.24 are compared with the present results in figure 8. Here, the spectra are presented in normalized form using the convective wavenumber. A value for the convective wavenumber was determined from the peak of the convective ridge in each case. The present results, where the variation of convection velocity with spatial separation is taken into account, show improved agreement with both the DNS and LES results at both superconvective and subconvective wavenumbers, in comparison to the constant convection velocity (Corcos) results. The Corcos result clearly overpredicts the levels at subconvective and low wavenumbers. A value of -0.145 for the decay constant at this frequency was found to yield the best agreement with the numerical results, which is consistent with the cross-spectral measurements of Farabee and Casarella (1991) at this frequency.
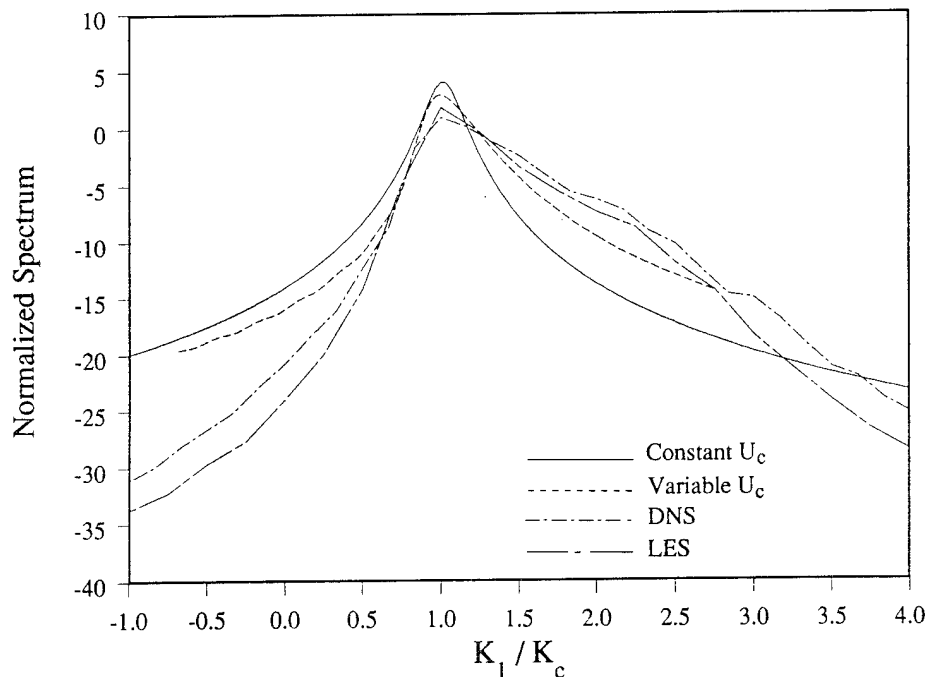


Figure 8. Comparison With "DNS" and "LES" Numerical Results

# ESTIMATED TWO-WAVENUMBER-FREQUENCY SPECTRUM $\Phi^*(K_1,K_2,\Omega)$

Thus far, we have focused on the wavenumber-frequency spectrum $\Phi^*(K_1,\Omega)$, which represents an integral over all spanwise wavenumbers $K_2$. The two-wavenumber-frequency spectrum $\Phi^*(K_1,K_2,\Omega)$ provides the distribution of energy in $K_2$ as well as in $K_1$. In particular, an estimation of $\Phi^*(K_1,K_2,\Omega)$ is required to determine the effects of finite-sized sensors on measured spectra. A two-dimensional array of pressure sensors is required to make a direct measurement of $\Phi^*(K_1,K_2,\Omega)$ or to make cross-spectral measurements from which $\Phi^*(K_1,K_2,\Omega)$ may be estimated. The Corcos model for the full cross spectrum may be expressed as

$$G(X,Z,\Omega) = \Phi(\Omega)e^{(\gamma|\Omega X/U_{c1}|-i(\Omega X/U_{c1}))}e^{(\beta|\Omega Z/U_{c2}|)} , \tag{8}$$

where $\beta$ is the spanwise decay constant. The normalized nondimensional wavenumber-frequency spectrum is then given by

$$\Phi^*(K_1,K_2,\Omega) = \int_{-\infty}^{\infty} \int_{-\infty}^{\infty} e^{(\gamma|\Omega X/U_{c1}|-i(-K_1 + \Omega/U_{c1})X)}e^{(\beta |\Omega Z/U_{c2}|i(K_2 Z))}dXdZ , \tag{9}$$

which with $U_{c1} = U_{c2} = \Omega/K_c$ ($U_{c1}$ and $U_{c2}$ are assumed to be independent of X and Z) may be evaluated in closed form to obtain

$$\Phi^*(K_1,K_2,\Omega) = 4\gamma\beta/((K_c^2(\gamma^2 + (1 - K_1/K_c)^2))(\beta^2 + (K_2/K_c)^2)) . \tag{10}$$

The spectra obtained from equation (10) for fixed frequencies $\Omega = 0.1, 1.0,$ and $10.0$ are shown in figure 9, where a value of 0.85 valid for large separations was taken for $U_c$, with $\gamma = -0.125$ and $\beta = -0.70$. In this analysis, we have not attempted to take into account the dependence of $U_{c1}$ and $U_{c2}$ or $\gamma$ and $\beta$ on frequency, as we are primarily interested in determining the effects of the variation of convection velocity alone on the spectra. The value taken for $\beta$ was based upon the measurements of Willmarth and Roos (1965). The spectra are normalized in wavenumber and spectral level using the convective wavenumber, which was defined at each frequency to be the streamwise wavenumber at which the spectrum $\Phi^*(K_1,\Omega)$ reached a global maximum. The spectra are symmetric about the convective peak in $K_1$ and about the origin in $K_2$. With increasing frequency, the spectral peaks decrease in magnitude and the distribution of energy becomes broader in wavenumber.

13

Equation (9) was evaluated with $U_{c1} = a(X+1)^b$ (where a and b are as previously defined) and $U_{c2} = 0.85$ for all frequencies. There are presently insufficient experimental and numerical data to determine the effectiveness of different forms for $U_{c2}$ for collapsing cross-spectral data. The absence of a mean spanwise convection velocity means that $U_{c2}$ represents a scaling parameter rather than a measurable quantity, as in the case of $U_{c1}$. Here we consider only a constant value of 0.85 for $U_{c2}$. For frequencies $\Omega = 0.1$ and 1.0, the convective peak displays a significant asymmetry in $K_1$, over a broad range of $K_2$, as shown in figure 10. This effect is not as apparent at the highest frequency, $\Omega = 10.0$. The convection velocity $U_{c1}$ enters only through the similarity variable $\Omega X/U_{c1}$. At higher frequencies, the effect of the variation of $U_{c1}$ with separation on the spectra is therefore diminished due to the increasing values of $\Omega$.

## CORRECTIONS TO AUTOSPECTRA MEASURED WITH CIRCULAR SENSORS

Corcos (1963) derived an expression for the ratio of the measured to the true autospectrum $\Phi_m(\omega)/\Phi_t(\omega)$ by formulating the problem in the spatial domain. The spatial formulation leads to the attenuation function

$$\Phi_m(\omega)/\Phi_t(\omega) = \int_{-\infty}^{\infty} \int_{-\infty}^{\infty} e^{(\gamma|\omega\xi/u_{c1}(\xi,\eta,\omega)|-i\omega\xi/u_{c1}(\xi,\eta,\omega))} e^{(\beta|\omega\eta/u_{c2}(\xi,\eta,\omega)|)}$$

$$T(\xi,\eta)d\xi d\eta \, , \tag{11}$$

where the sensor spatial correlation function is given for a circular sensor of radius r by

$$T(\xi,\eta) = \{2/\pi r^2\}\{\cos^{-1}(\varepsilon/2r)-(\varepsilon/2r)(1 - (\varepsilon/2r)^2)^{1/2}\}, \qquad \varepsilon/2r \leq 1 \, ,$$

$$T(\xi,\eta) = 0 \, , \qquad\qquad\qquad\qquad\qquad\qquad \varepsilon/2r > 1 \, ,$$

and

$$\varepsilon = (\xi^2+\eta^2)^{1/2} \, . \tag{12}$$

Here we have considered the most general case, allowing $u_{c1}$ and $u_{c2}$ to vary with $\xi$, $\eta$, and $\omega$. In this case, equation (11) cannot be evaluated in closed form and requires numerical integration. In view of equation (12), the limits of integration for equation (11) must extend only over the region bounded by $\varepsilon/2r <= 1$. For this reason, the spatial formulation is computationally less intensive than the analogous wavenumber formulation.

14
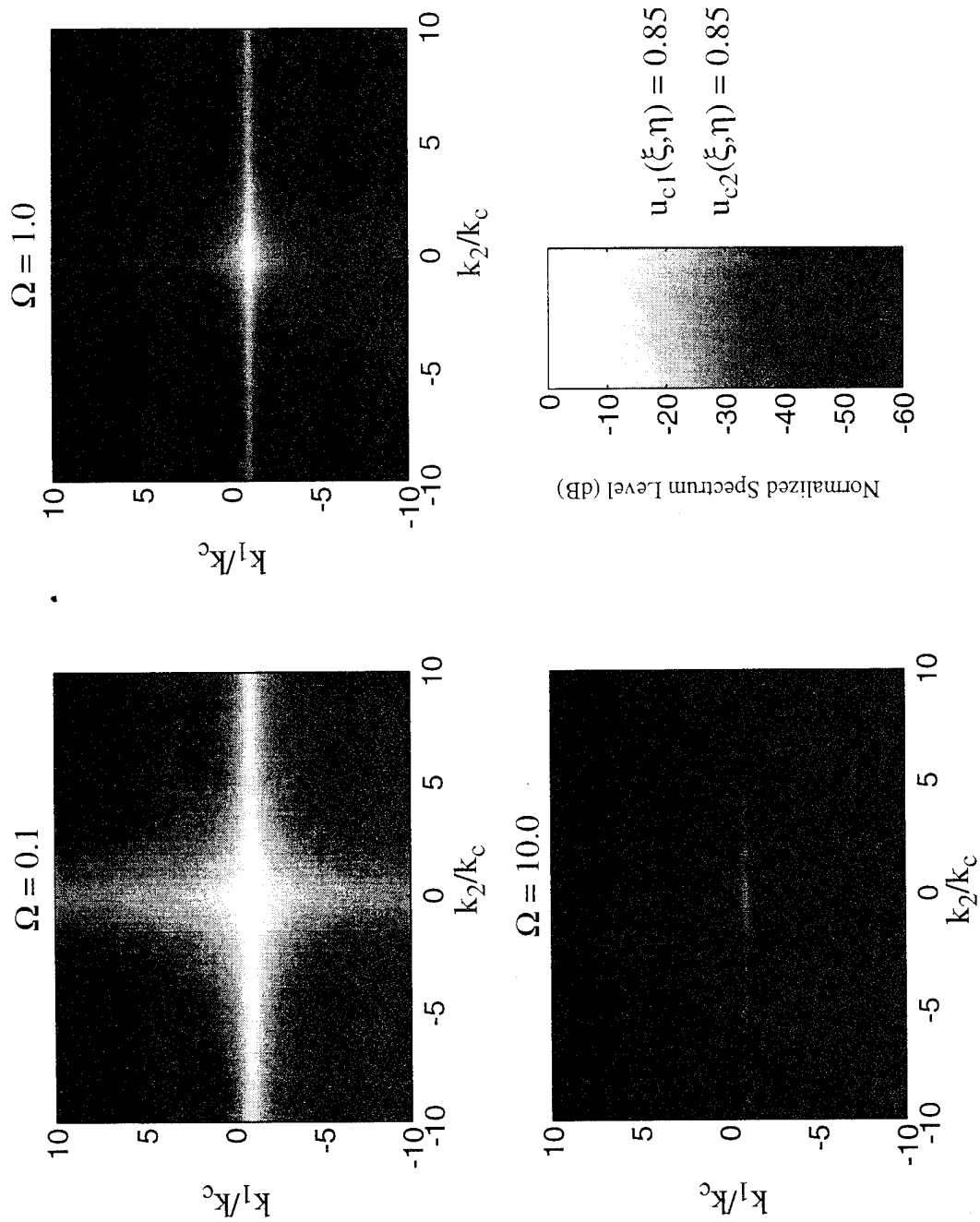
Figure 9. Computed Wavenumber-Frequency Spectrum $\Phi_a^*(K_1, K_2, \Omega)$ for $u_{c1} = u_{c2} = 0.85$

Figure 10. Computed Wavenumber-Frequency Spectrum $\Phi_b*(K_1, K_2, \Omega)$ for $u_{c1}(\xi) = a(\xi+1)^b$ and $u_{c2}(\eta) = a(\eta+1)^b$

$u_{c1}(\xi,\eta) = a(|\xi|+1)^b$, $|\xi| < \xi_m$
$u_{c2}(\xi,\eta) = a(|\eta|+1)^b$, $|\eta| < \eta_m$
where $\xi_m = \eta_m = (0.85/a)^{1/b} - 1$
$a = 0.6453$
$b = 0.0627$

$\Omega = 1.0$

$\Omega = 0.1$

$\Omega = 10.0$

$k_1/k_c$

$k_2/k_c$

Normalized Spectrum Level (dB)

16

In formulating his results, Corcos assumed $u_c$ was independent of spatial separation, but could vary with frequency. For that case, with $u_{c1}(\xi,\eta,\omega) 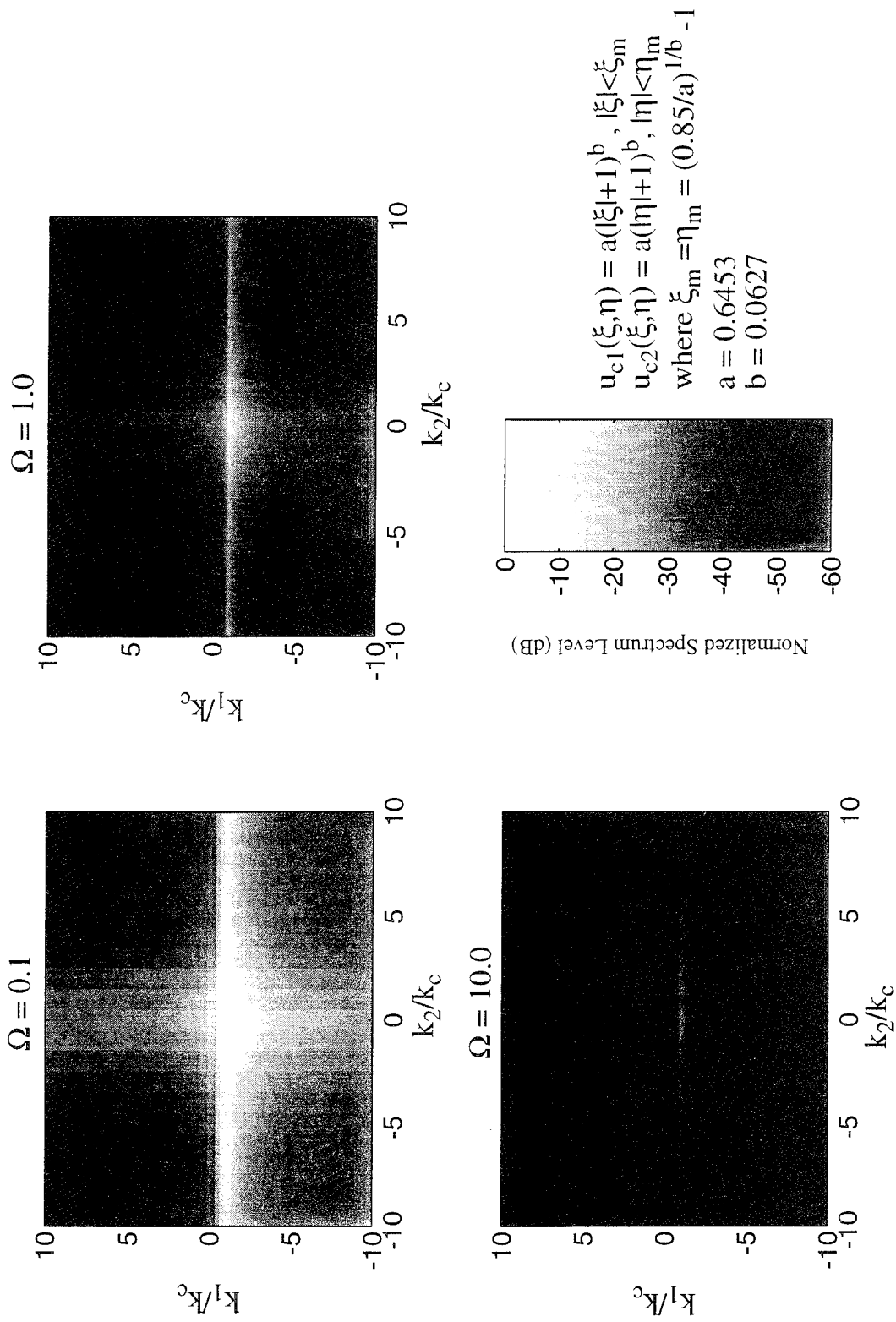= u_{c2}(\xi,\eta,\omega) = u_c(\omega)$ and application of a change of variables in equation (11), the attenuation $\Phi_m(\omega)/\Phi_t(\omega)$ may be shown to depend only upon the quantity $\omega r/u_c(\omega)$. The attenuations may therefore be computed in terms of the variable $\omega r/u_c(\omega)$, without specifying a particular form for $u_c(\omega)$. Our results were computed with a constant value of -0.125 for $\gamma$ and -0.70 for $\beta$ in equation (11). We therefore have not attempted to take into account the dependence of $\gamma$ and $\beta$ on frequency. The slightly higher levels in comparison to those of Corcos (1963), as shown in figure 11, are thought to result from the values for $\gamma$ and $\beta$ used by Corcos (not stated) and possibly the computational methods.

We are primarily interested in determining if the variation of convection velocity with separation has a significant effect on the attenuations in the frequency spectrum. In the previous section, we determined $\Phi^*(K_1,K_2,\Omega)$ at three discrete frequencies and did not attempt to take into account the variation of convection velocity with frequency. Here we estimate the attenuations over a continuous range of frequencies. We therefore formulate equation (11) so as to express the attenuations in terms of $\omega r/u_{co}(\xi_o,\eta_o,\omega)$ with $u_{co}(\xi_o,\eta_o,\omega)$ an arbitrarily chosen "reference" convection velocity, which may vary with frequency. We further make the simplifying assumption that the convection velocities are separable in frequency and space, such that
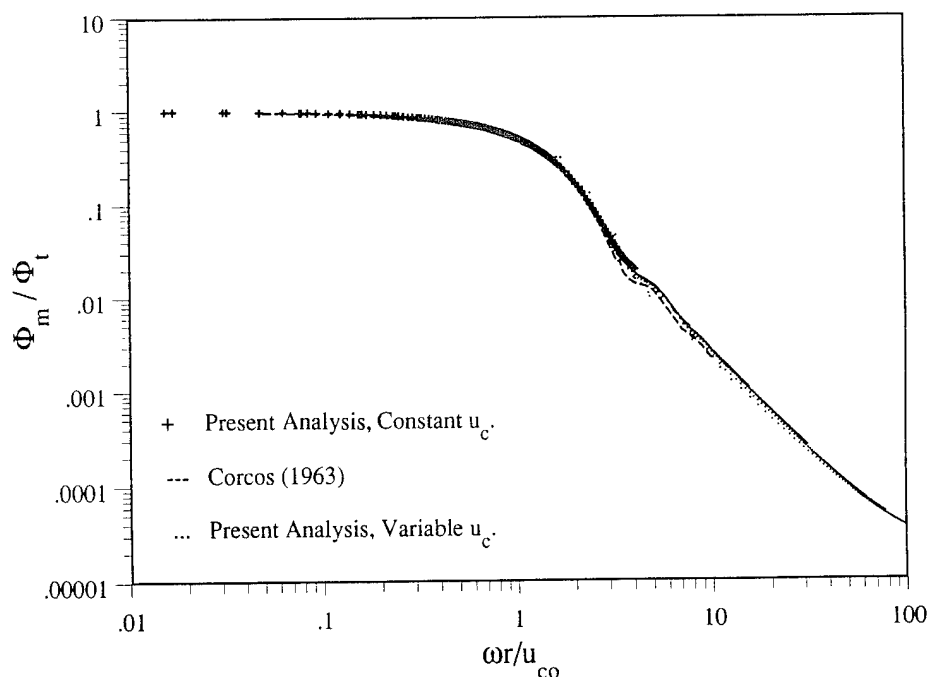


Figure 11. Autospectrum Attenuations for Constant and Spatially Varying Convection Velocity

$$u_{c1}(\xi,\eta,\omega) = g(\omega)h_1(\xi,\eta) ,$$

$$u_{c2}(\xi,\eta,\omega) = g(\omega)h_2(\xi,\eta) .$$

(13)

Although there is insufficient experimental data to rigorously justify this assumption, the results of Abraham (1994) obtained from the DNS channel flow database (see Choi and Moin (1990)) suggest a separable form for $u_{c1}(\xi,\omega)$. We also assume the same frequency dependence, $g(\omega)$, holds for both functions.

We define a transformation of variables given by

$$x = \xi/r , \qquad z = \eta/r , \qquad \omega^* = \omega r/u_{co}(\xi_o,\eta_o,\omega) ,$$

such that equation (11) becomes

$$\Phi_m(\omega)/\Phi_t(\omega) = \int_{-\infty}^{\infty} \int_{-\infty}^{\infty} e^{(\gamma|\omega^* x h(x_o,z_o)/h(x,z)| - i\omega^* x h(x_o,z_o)/h(x,z))}$$

$$e^{(\beta|\omega^* z h(x_o,z_o)/h(x,z)|)} T^*(x,z) dx dz .$$

(14)

With this transformation, $T^*(x,z)$ does not depend explicitly upon $r$, and for any $h(x,z)$ and $h(x_o,z_o)$, the attenuation depends only upon the quantity $\omega^*$. Here, the attenuation depends implicitly on the frequency dependence of the convection velocity, $g(\omega)$, only through the variable $\omega^*$. We arbitrarily choose $h(x_o,z_o) = h(0,0) = 0.645U_o$. We assume that $u_{c1}(\xi,\eta,\omega) = u_{c1}(\xi,\omega)$ and $u_{c2}(\xi,\eta,\omega) = u_{c2}(\eta,\omega)$ such that the cross spectrum retains a separable form, with $h_1(\xi) = a(\xi + 1)^b$ and $h_2(\eta) = a(\eta + 1)^b$ and with a and b as previously defined. In this case, there was no measurable change in the attenuation function with respect to the former results, as shown in figure 11. The computed attenuations for six different values of $r/\delta^*$ collapse onto a single curve when scaled with $\omega^*$, consistent with the formulation given by equation (14). The change in slope for $\omega r/u_{co} \sim 4$ reflects the first zero in the wavenumber response of the circular pressure sensor.

The interpretation of the effects of sensor size on attenuations in the autospectrum is aided by formulating the problem in the wavenumber domain, as shown by Keith and Bennett (1991). Here, the redistribution of energy with wavenumber, as shown to occur in figure 10, is insufficient to significantly affect the attenuations in the autospectrum, due to the inherent averaging over all

18

wavenumbers resulting from the sensor. The increases and decreases in levels are therefore effectively canceled by the wavenumber response of the sensor.

## CONCLUSIONS

Comparison of convection velocities from experimental measurements and from numerical simulations covering two orders of magnitude in $R_\theta$ supports an outer variable scaling for collapsing the data. The early work of Corcos provided a model for the wall pressure cross spectrum in terms of a similarity scaling based upon a convection velocity assumed independent of spatial separation. Recent measurements still support this similarity scaling, with the dependence of $u_c$ on spatial separation taken into account. An improvement in the wavenumber-frequency spectrum $\Phi^*(K_1,\Omega)$ estimated from the cross spectrum is obtained by including this effect when computing the spatial Fourier transform, as evidenced by the favorable comparison with recent numerical results. The redistribution of energy in wavenumber resulting from the spatial variation of the convection velocity did not affect the attenuations in the autospectra, due to the inherent averaging over all wavenumbers by the sensor.

In view of the sensitivity of the estimated spectrum to the convection velocity and also the decay constants, the limited cross-spectral data presently available preclude formulating a model for the wavenumber-frequency spectrum valid over a wide range of frequencies as well as Reynolds numbers. We have used Farabee and Casarella's measurements, which provide the most extensive set of streamwise cross-spectral data. For applied problems of flow-induced vibration and noise, estimates of the wall pressure wavenumber-frequency spectrum may be determined numerically by use of the methods presented here, taking into account effects related to the particular frequencies and Reynolds numbers of interest. Although we have used convection velocity data here, the actual phase data will improve the accuracy.

# REFERENCES

Abraham, B. M., 1994, "Identification of the Wavenumber Content of High Magnitude Pressure Events Beneath a Turbulent Boundary Layer," Master of Science Thesis, University of Connecticut, Storrs, CT, 1994.

Bull, M. K., 1967, "Wall-Pressure Fluctuations Associated With Subsonic Turbulent Boundary Layer Flow," *Journal of Fluid Mechanics*, Vol. 28, Part 4, pp. 719-754.

Chang, P.A., Abraham, B. M., and Piomelli, U., 1994, "Wavenumber-Frequency Characteristics of Wall Pressure Fluctuations Computed Using Turbulence Simulations," *Proceedings of the ASME Symposium on the Active Control of Vibration and Noise*, DE-Vol. 75.

Choi, H., and Moin, P., 1990, "On the Space-Time Characteristics of Wall-Pressure Fluctuations," *Physics of Fluids* (A) 2 (8), August, pp. 1450-1460.

Corcos, G. M., 1963, "Resolution of Pressure in Turbulence," *Journal of the Acoustical Society of America*, Vol. 35, No. 2, February, pp. 192-199.

Farabee, T. M., 1986, "An Experimental Investigation of Wall Pressure Fluctuations Beneath Non-Equilibrium Turbulent Flows," Report No. DTNSRDC-86/047, David Taylor Naval Ship Research & Development Center, Bethesda, MD, May.

Farabee, T. M. and Casarella, M. J., 1991, "Spectral Features of Wall Pressure Fluctuations Beneath Turbulent Boundary Layers," *Physics of Fluids* A 3 (10), October.

Keith, W. L., 1989, "Spectral Measurements of Pressure Fluctuations on Riblets," *Journal of the AIAA* (TN), Vol. 27, No. 12, pp. 1822-1824, December.

Keith, W. L., and Abraham, B. M., 1994, "Derivation of a Wavenumber Filter Design for the Measurement of Turbulent Wall Pressure Fluctuations," *Proceedings of the ASME Symposium on Application of Microfabrication to Fluid Mechanics*, FED-Vol. 197, Chicago, IL, 6-11 November.

Keith, W. L., and Bennett, J. C., 1991, "Correction of Wall Pressure Fluctuation Measurements With a View to Hydrodynamic Applications," *Proceedings of the ASME Forum on Turbulent Flows*, FED-Vol. 112, Portland OR, 23-27 June.

Keith, W. L., Bennett, J. C., and Barclay, J. J., 1991, "Hydroacoustic Research at the Quiet Water Tunnel Facility of the Naval Underwater Systems Center," *Proceedings of the ASME Symposium on Hydroacoustic Facilities*, NCA-Vol.10, Atlanta, 1-6 December.

Keith, W. L., and Barclay, J. J., 1993, "Effects of a Large Eddy Breakup Device on the Fluctuating Wall Pressure Field," *Journal of Fluids Engineering*, Vol. 115, No. 3, September, pp. 389-397.

Rand, R. H., 1984, "Computer Algebra in Applied Mathematics: An Introduction to MACSYMA," Pitman, MA.

Schloemer, H. H., 1967, "Effects of Pressure Gradients on Turbulent-Boundary-Layer Wall-Pressure Fluctuations," *Journal of the Acoustical Society of America*, Vol. 42, No. 1, pp. 93-113, July.

# REFERENCES (CONT'D)

Willmarth, W. W., and Roos, F. W., 1965, "Resolution and Structure of the Wall Pressure Field Beneath a Turbulent Boundary Layer," *Journal of Fluid Mechanics*, Vol. 22, No. 1, pp. 81-94.

Willmarth, W. W., and Wooldridge, C. E., 1962, "Measurements of the Fluctuating Pressure at the Wall Beneath a Thick Turbulent Boundary Layer," *Journal of Fluid Mechanics*, Vol. 14, No. 2, pp. 187-210.

# INITIAL DISTRIBUTION LIST

| Addressee | No. of Copies |
|---|---|
| Defense Technical Information Center | 12 |
| U.S. Coast Guard Academy | |
| (K. Colella) | 1 |
| Office of Naval Research | |
| (Dr. L. P. Purtell) | 1 |
| (Dr. K. Ng) | 1 |
| Naval Surface Warfare Center, Carderock Division | |
| (Dr. T. Farabee) | 1 |